Concentration-Dependent Induction of Reactive Oxygen Species, Cell Cycle Arrest and Apoptosis in Human Liver Cells After Nickel Nanoparticles Exposure

Javed Ahmad,[1] Hisham A. Alhadlaq,[2,3] Maqsood A. Siddiqui,[1] Quaiser Saquib,[1] Abdulaziz A. Al-Khedhairy,[1] Javed Musarrat,[4] Maqusood Ahamed[2]

[1]Department of Zoology, College of Science, King Saud University, Riyadh 11451, Saudi Arabia

[2]King Abdullah Institute for Nanotechnology, King Saud University, Riyadh 11451, Saudi Arabia

[3]Department of Physics and Astronomy, College of Science, King Saud University, Riyadh 11451, Saudi Arabia

[4]Department of Agricultural Microbiology, Faculty of Agricultural Sciences, Aligarh Muslim University, Aligarh 202002, India

Received 1 April 2013; revised 21 May 2013; accepted 22 May 2013

ABSTRACT:: Due to advent of nanotechnology, nickel nanoparticles (Ni NPs) are increasingly recognized for their utility in various applications including catalysts, sensors and electronics. However, the environmental and human health effects of Ni NPs have not been fully investigated. In this study, we examined toxic effects of Ni NPs in human liver (HepG2) cells. Ni NPs were prepared and characterized by X-ray diffraction, transmission electron microscopy and dynamic light scattering. We observed that Ni NPs (size, ~28 nm; concentration range, 25–100 μg/mL) induced cytotoxicity in HepG2 cells and degree of induction was concentration-dependent. Ni NPs were also found to induce oxidative stress in dose-dependent manner evident by induction of reactive oxygen species and depletion of glutathione. Cell cycle analysis of cells treated with Ni NPs exhibited significant increase of apoptotic cell population in subG1 phase. Ni NPs also induced caspase-3 enzyme activity and apoptotic DNA fragmentation. Upregulation of cell cycle checkpoint gene p53 and bax/bcl-2 ratio with a concomitant loss in mitochondrial membrane potential suggested that Ni NPs induced apoptosis in HepG2 cells was mediated through mitochondrial pathway. This study warrants that applications of Ni NPs should be carefully assessed as to their toxicity to human health. Environ Toxicol 00: 000–000, 2013.

Keywords: nickel nanoparticles; human liver cells; health effects; oxidative stress; cell cycle

Correspondence to: M. Ahamed; e-mail: maqusood@gmail.com

Contract grant sponsor: King Abdulaziz City for Science and Technology (KACST), Riyadh, Saudi Arabia (National Plan for Science and Technology (NPST)).

Contract grant number: 10-NAN1201-02.

Published online 0 Month 2013 in Wiley Online Library (wileyonlinelibrary.com). DOI: 10.1002/tox.21879

INTRODUCTION

Metallic nickel (Ni) and Ni compounds are released into the atmosphere during mining, smelting, and refining operations representing an environmental and industrial pollutant (Cavallo et al., 2003; Magaye and Zhao, 2012). Evidence

indicates that various Ni compounds cause pulmonary inflammation, fibrosis, emphysema, and cancer (Oller et al., 1997). Studies in experimental animals suggest that metallic Ni is reasonably anticipated to be a human carcinogen (Sivulka, 2005). The International Agency for Research on Cancer (IARC), therefore, classed Ni compounds as group 1: carcinogenic to humans, while metallic Ni is classed as group 2B: possibly carcinogenic to humans (Kasprzak et al., 2003).

Recently, another type of exposure to metallic Ni, becoming more important with increased use, is in the form of nanoparticles (NPs) (Clancy and Costa, 2012). Ni NPs is a product with many new characteristics, which include a high level of surface energy, high magnetism, low melting point, low burning point, and high surface area. These characteristics are only present at the nanoscale level and have thus led to its heightened experimentation and use in modern industries such as catalysts, sensors, and electronic applications (Zhang et al., 2003). However, these same properties of Ni NPs may present unique potential health impact (Andrew and Maynard, 2005). The nano size of these particles renders them the ability to be easily transported into biological systems, thus raising the question of their effects on the susceptible system. Therefore, scientific research on the environmental and human health effects of Ni NPs is imperative (Magaye and Zhao, 2012).

There are few important studies showing the toxicity of Ni NPs. Zhao et al. (2009) observed that Ni NPs induced apoptosis in mouse epidermal JB6 cells through a caspase-8/AIF mediated cytochrome c-independent pathway. Cytotoxic effect of Ni NPs on leukemia cancer cells was also reported by Guo et al. (2008). Ispas et al. (2009) have shown that the effect of Ni NPs sized at 30, 60, and 100 nm as well as aggregated particle clusters of 60 nm having dendritic structures were delivered to zebrafish embryos to assess changes in mortality and developmental defects. Our previous study demonstrated that Ni NPs induce oxidative stress mediated apoptosis in human lung epithelial (A549) cells (Ahamed, 2011). However, none of the investigations, so far, have explored toxic effects of Ni NPs in human liver, which is the primary organ of metabolism. Studies suggest that NPs may be absorbed as they pass through the gastrointestinal tract and distributed to different organs like liver via the circulatory system. Researchers have shown that the NPs when orally administered to mice accumulate in liver and cause toxicity (Chen et al., 2007; Wang et al., 2008). Kim et al. (2008) also examined the oral toxicity of silver NPs in rats and found significant dose-dependent changes in alkaline phosphatase activity, cholesterol level and liver function. NPs can be delivered into the gastrointestinal tract via accidental ingestion by individuals who work in the NPs manufacturing industry or NPs research laboratories or by drinking or eating water or food that is contaminated by NPs.

This study was designed to examine the cytotoxic effect of Ni NPs using human liver (HepG2) cell line. Furthermore, reactive oxygen species (ROS), glutathione (GSH), mitochondrial membrane potential (MMP), expression of apoptotic genes, caspase-3 activity, and DNA fragmentation along with cell cycle analysis were also investigated to reveal possible mechanisms of toxicity caused by exposure to Ni NPs. We have chosen liver cell line because liver organ might act as a major target organ for NPs after they gain entry into the body through any of the possible routes. HepG2 cell line retains the functions of fully differentiated primary hepatocytes and widely used as a model system for hepatotoxicity studies (Zou et al., 2011; Ahmad et al., 2012, Sharma et al., 2012). Ni NPs were prepared by a reduction method using hydrate hydrazine as a reducing agent. Synthesized Ni NPs were characterized by transmission electron microscopy (TEM), X-ray diffraction (XRD), and dynamic light scattering (DLS).

MATERIALS AND METHODS

Reagents

Dulbecco's modified eagle's medium (DMEM), hank's balanced salt solution (HBSS), fetal bovine serum (FBS), penicillin-streptomycin and trypsin were purchased from Invitrogen (Carlsbad, CA). MTT [3-(4,5-2-yl)-2,5-diphenyltetrazoliumbromide], 2,7-dichlorofluorescin diacetate (DCFH-DA), glutathione (GSH) and Rhodamine-123 dye (Rh123) were obtained from Sigma-Aldrich (St. Louis, MO). Kits for caspase-3 enzyme and DNA ladder were bought from BioVision (USA) and Roche (USA), respectively. All other chemicals used were of the highest purity available from commercial sources.

Synthesis of Nickel Nanoparticles

Ni NPs were synthesized through a solution reduction process using hydrate hydrazine as a reducing agent as described by Wang et al. (2008). First, hydroxyethyl carboxymethyl cellulose (HECMC) was added to the solution of $NiCl_2.6H_2O$ (0.2 wt %). Then NaOH solution and hydrate hydrazine was added into the above mixture until the pH value was about 11. The resulting solution was kept in a thermostatic bath until black powder precipitated completely. Finally, the product was washed with distilled water and ethanol for several times, and then dried in a vacuum drying oven at room temperature to get dry powder of Ni NPs.

Characterization of Nickel Nanoparticles

The crystalline nature of Ni NPs was carried out by taking XRD pattern. The XRD of Ni NPs was acquired at room temperature with the help of PANalytical X'Pert X-ray diffractometer equipped with a Ni filter using Cu K_α ($\lambda = 1.54056$ Å) radiations as X-ray source. Shape and size

of Ni NPs were determined by field emission transmission electron microscopy (FETEM, JEM-2100F, JEOL, Japan) at an accelerating voltage of 200 kV. Hydrodynamic diameter and zeta potential of Ni NPs in aqueous solution (culture medium) was determined by DLS (Nano-Zetasizer-HT, Malvern Instruments, Malvern, UK) as described by Murdock et al. (2008).

Cell Culture and Nickel Nanoparticles Treatment

HepG2 cells were obtained from American Type Culture Collection (ATCC) (Manassas, VA). Cells were used between passages 10–20. Cells were cultured in MEM medium supplemented with 10% FBS, 100 U/mL penicillin-streptomycin, 1 mM sodium pyruvate, and 1.5 g/L sodium bicarbonate at 5% CO_2 and 37°C. At 85% confluence, cells were harvested using 0.25% trypsin and were sub-cultured. Cells were allowed to attach the surface for 24 h prior to NPs exposure. Ni NPs were suspended in cell culture medium and diluted to appropriate concentrations (1–100 μg/mL). The dilutions of Ni NPs were then sonicated using a sonicator bath at room temperature for 15 min at 40 W to avoid NPs agglomeration prior to administration to the cells. Cells not exposed to Ni NPs served as control in each experiment.

MTT Assay

MTT assay was carried out following the procedure as described by Mossman (1983) with some modifications (Ahamed et al., 2011). The MTT assay assesses the mitochondrial function by measuring ability of viable cells to reduce MTT into blue formazon product. In brief, 1×10^4 cells/well were seeded in 96-well plates and exposed to different concentrations of Ni NPs (1–100 μg/mL) for 24 h. At the end of exposure, medium was removed from each well to avoid interference of NPs and replaced with new medium containing MTT solution in an amount equal to 10% of culture volume, and incubated for 3 h at 37°C until a purple colored formazan product developed. The resulting formazan product was dissolved in acidified isopropanol. Furthermore, the 96-well plate was centrifuged at 2300 × *g* for 5 min to settle down the remaining NPs present in the solution. Then, a 100 μL supernatant was transferred to other fresh wells of 96-well plate and absorbance was measured at 570 nm by using a microplate reader (Synergy-HT, BioTek).

NRU Assay

Neutral red uptake (NRU) assay was performed following the procedure as described by Borenfreund and Puerner (1984) with some modifications (Ahamed et al., 2011). In brief, 1×10^4 cells/well were seeded in 96-well plates and exposed to different concentrations of Ni NPs (1–100 μg/mL) for 24 h. At the end of exposure, test solution was aspirated and cells were washed with phosphate buffer saline (PBS) twice and incubated for 3 h in medium supplemented with neutral red (50 μg/mL). The medium was washed off rapidly with a solution containing 0.5% formaldehyde and 1% calcium chloride. Cells were further incubated for 20 min at 37°C in a mixture of acetic acid (1%) and ethanol (50%) to extract the dye. Further, 96-well plate was centrifuged at 2300 × *g* for 5 min to settle down the remaining NPs present in the solution. Then, a 100 μL supernatant was transferred to other fresh wells of 96-well plate and absorbance was measured at 540 nm by using a microplate reader (Synergy-HT, BioTek).

Measurement of Intracellular Reactive Oxygen Species Generation

The production of intracellular ROS was measured using 2,7-dichlorofluorescin diacetate (DCFH-DA) as described by Wang and Joseph (1999) with some modifications (Siddiqui et al., 2010). The DCFH-DA passively enters the cell where it reacts with ROS to form the highly fluorescent compound dichlorofluorescein (DCF). In brief, HepG2 cells (5×10^4) were seeded in six-well plates and allowed for adherence. Cells were exposed to different concentrations of Ni NPs (25–100 μg/mL) for 24 h. Following exposure, cells were washed twice with PBS and incubated for 30 min in dark in culture medium (without FBS) containing DCFH-DA (20 μM). The control and treated cells were visualized by use of a fluorescence microscope (OLYMPUS CKX 41) by grabbing the images at 20× magnification.

Preparation of Crude Cell Extract

We have prepared the crude cell extract for GSH and caspase-3 enzyme assays. Briefly, cells were exposed to different concentrations of Ni NPs (25–100 μg/mL) for 24 h. At the end of exposure, control and exposed cells were harvested in ice-cold phosphate buffer saline by scraping and washed with phosphate buffer saline at 4°C. The cell pellets were then lysed in cell lysis buffer [1 × 20 mM Tris-HCl (pH 7.5), 150 mM NaCl, 1 mM Na_2EDTA, 1% Triton, 2.5 mM sodium pyrophosphate] as described in our previous publication (Ahmad et al., 2012). Following centrifugation (10,000 × *g* for 10 min at 4°C) the supernatant (crude cell extract) was maintained on ice.

Intracellular Glutathione Assay

GSH level was determined as described by Chandra et al. (2002) with some specific modifications (Ahamed et al., 2011). Briefly, cellular proteins were precipitated by incubating 1 mL of crude cell extract with 1 mL TCA (10%) and placed on ice for 1 h following by a 10 min centrifugation at 3000 rpm. The supernatant was added to 2 mL of 0.4 M Tris buffer (pH 8.9) containing 0.02 M EDTA followed by an addition of 0.01 M 5,50-dithionitrobenzoic acid (DTNB) to

a final volume of 3 mL. The tubes were incubated for 10 min at 37°C in water bath with shaking. The absorbance of yellow color developed was read at 412 nm using multiplate reader (Synergy HT, Bio-Tek, USA).

Assay of Mitochondrial Membrane Potential

Mitochondrial membrane potential (MMP) was measured following the protocol of Zhang et al. (2011) with some modifications (Siddiqui et al., 2010). In brief, control and treated cells were harvested and washed twice with PBS. Cells were further exposed with 10 μg/mL of Rh-123 fluorescent dye for 1 h at 37°C in dark. Again cells were washed twice with PBS. Then, fluorescence intensity of Rh-123 dye was measured using upright fluorescence microscope (OLYMPUS CKX 41) by grabbing the images at 20× magnification.

Flow Cytometric Analysis of Cell Cycle Progression

Cells treated with different concentrations (25–100 μg/mL) of Ni NPs for 24 h were harvested and entrifuged at 1000 × *g* for 4 min. Pellets were re-suspended in 500 μL of PBS. Cells were fixed with equal volume of chilled 70% ice-cold ethanol, and incubated at 4°C for 1 h. After two successive washes with PBS at 1000 rpm for 4 min, cell pellets were re-suspended in PBS and stained with 50 μg propiodium iodide (PI)/mL containing 0.1% Triton X-100 and 0.5 mg/mL RNAase A for 1 h at 30°C in dark. Fluorescence of the PI was measured by flow cytometry by use of a Beckman Coulter flow cytometer (Coulter Epics XL/Xl-MCL, Miami, USA) through a FL-4 filter (585 nm) and 10,000 events were acquired (Darzynkiewicz et al., 1992). The data were analyzed by Coulter Epics XL/XL-MCL, System II Software, Version 3.0. Cell debris was characterized by a low FSC/SSC was excluded from the analysis.

Total RNA Isolation and Quantitative Real-Time PCR Analysis

Cells were exposed to different concentrations (25–100 μg/mL) of Ni NPs for 24 h. At the end of exposure, total RNA was extracted by RNeasy mini Kit (Qiagen,Valencia, CA) according to the manufacturer's instructions. Concentration of the extracted RNA were determined using Nanodrop 8000 spectrophotometer (Thermo-Scientific, Wilmington, DE) and the integrity of RNA were visualized on 1% agarose gel using gel documentation system (Universal Hood II, BioRad, Hercules, CA). The first strand cDNA was synthesized from 1 μg of total RNA by Reverse Transcriptase using M-MLV (Promega, Madison, WI) and oligo (dT) primers (Promega) according to the manufacturer's protocol. Quantitative real-time PCR (RT-PCRq) was performed by QuantiTect SYBR Green PCR kit (Qiagen) using ABI PRISM 7900HT sequence detection system (Applied Biosystems, Foster City, CA). Two microliters of template cDNA was added to the final volume of 20 μL of reaction mixture. Real-time PCR cycle parameters included 10 min at 95°C followed by 40 cycles involving denaturation at 95°C for 15 s, annealing at 60°C for 20 s and elongation at 72°C for 20 s. The sequences of the specific sets of primer for p53, bax, bcl-2 and caspase-3 used in this study were given in our previous publication (Ahamed et al., 2011). Primer sequence of GAPDH gene was 5′F-GCTGCCTTCT CTTGTGACAAAGT-3′, 5′R-CTCAGCCTTGACTGTGCC ATT-3′. Expressions of selected genes were normalized to GAPDH gene, which was used as an internal housekeeping control. All the real-time PCR experiments were performed in triplicate and data expressed as the mean of at least three independent experiments.

Casapase-3 Enzyme Assay

Activity of caspase-3 enzyme was measured in treated and control cells using standard assay kit (BioVision). This assay is based on the principle that activated caspases in apoptotic cells cleave the synthetic substrates to release free chromophore p-nitroanilide (pNA), which is measured at 405 nm (Berasain et al., 2005; Ahamed et al., 2011). The pNA was generated after specific action of caspase-3 on tertrapeptide substrates DEVD-pNA. Briefly, reaction mixture consisted of 50 μL of cell extract protein (50 μg) (from control and Ni NPs treated cells), 50 μL of 2× reaction buffer (containing 10 mM dithiothreitol) and 5 μL of 4 mM DEVD-pNA substrate in a total volume of 105 μL. The reaction mixture was incubated at 37°C for 1 h and absorbance of the product was measured using microplate reader (Synergy-HT, BioTek) at 405 nm according to manufacturer's instruction.

DNA Fragmentation Assay

Apoptotic DNA fragmentation assay was performed in HepG2 cells exposed to different concentrations (25–100 μg/mL) of Ni NPs for 24 h. At the end of exposure, DNA was extracted using an apoptotic DNA Ladder Kit (Roche). The extracted DNA was then evaluated on a 1% agarose gel using ethidium bromide. DNA fragmentation pattern was documented by a gel documentation system.

Protein Estimation

The total protein content in cell extracts was estimated by the Bradford method (Bradford, 1976) using bovine serum albumin as standard.

Statistical Analysis

Statistical significance was determined by one-way analysis of variance (ANOVA) followed by Dunnett's multiple comparison test. Significance was ascribed at $p < 0.05$.

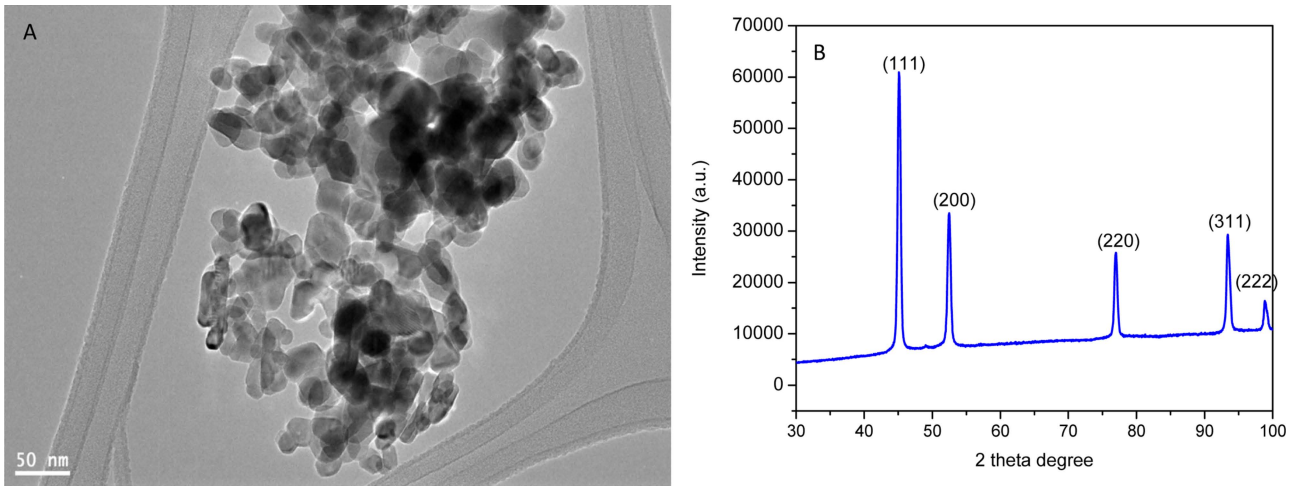

Fig. 1. Characterization of Ni NPs. (A) TEM and (B) XRD. [Color figure can be viewed in the online issue, which is available at wileyonlinelibrary.com.]

RESULTS

TEM, XRD, and DLS Characterization of Nickel Nanoparticles

Figure 1(A) shows the typical TEM image of Ni NPs. TEM average diameter was calculated from measuring over 100 particles in random fields of TEM view. The average TEM diameter of Ni NPs was 28.39 nm. Figure 1(B) shows the XRD pattern of Ni NPs that clearly exhibits the crystalline nature of this material. The crystallite size has been estimated from the XRD pattern using the Scherrer's equation (Patterson, 1939). The average crystallite size of Ni NPs was also found to be 27.98 nm supporting the TEM data. The mean hydrodynamic diameter and zeta potential of Ni NPs in cell culture medium determined by DLS was 278 nm and -19 mV, respectively.

Nickel Nanoparticles Decreased Cell Viability

Cells were exposed to Ni NPs at the concentrations of 0, 1, 2, 5, 10, 25, 50, and 100 μg/mL for 24 h and cell viability was determined using MTT and NRU assays. Both assays demonstrated that Ni NPs up to the concentration of 10 μg/mL, did not produce significant reduction in cell viability. As the concentration of NPs increased to 25, 50, and 100 μg/mL, reduction in cell viability was observed in concentration-dependent manner. In MTT assay, cell viability decreased to 81, 66, and 52% when cells exposed to Ni NPs at the concentrations of 25, 50, and 100 μg/mL, respectively [Fig. 2(A)]. Figure 2(B) shows the results of cell viability obtained by NRU assay. In NRU assay cell viability decreased to 85, 73, and 56% when cells exposed to Ni NPs at the concentrations of 25, 50, and 100 μg/mL, respectively.

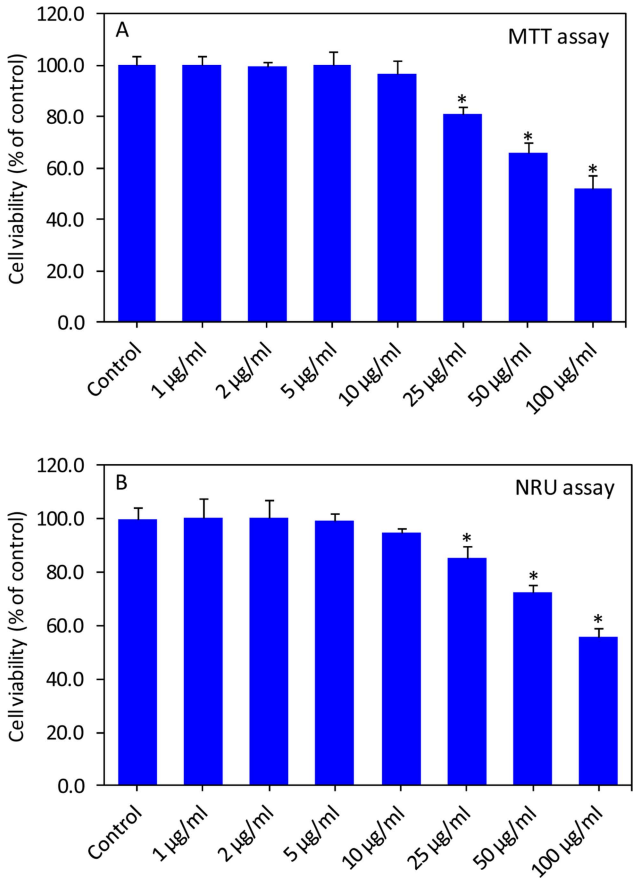

Fig. 2. Dose-dependent depletion of HepG2 cells viability after Ni NPs exposure. (A) MTT assay and (B) NRU assay. Data represented are mean±SD of three identical experiments made in three replicate. *Statistically significant difference as compared to control ($p < 0.05$). [Color figure can be viewed in the online issue, which is available at wileyonlinelibrary.com.]

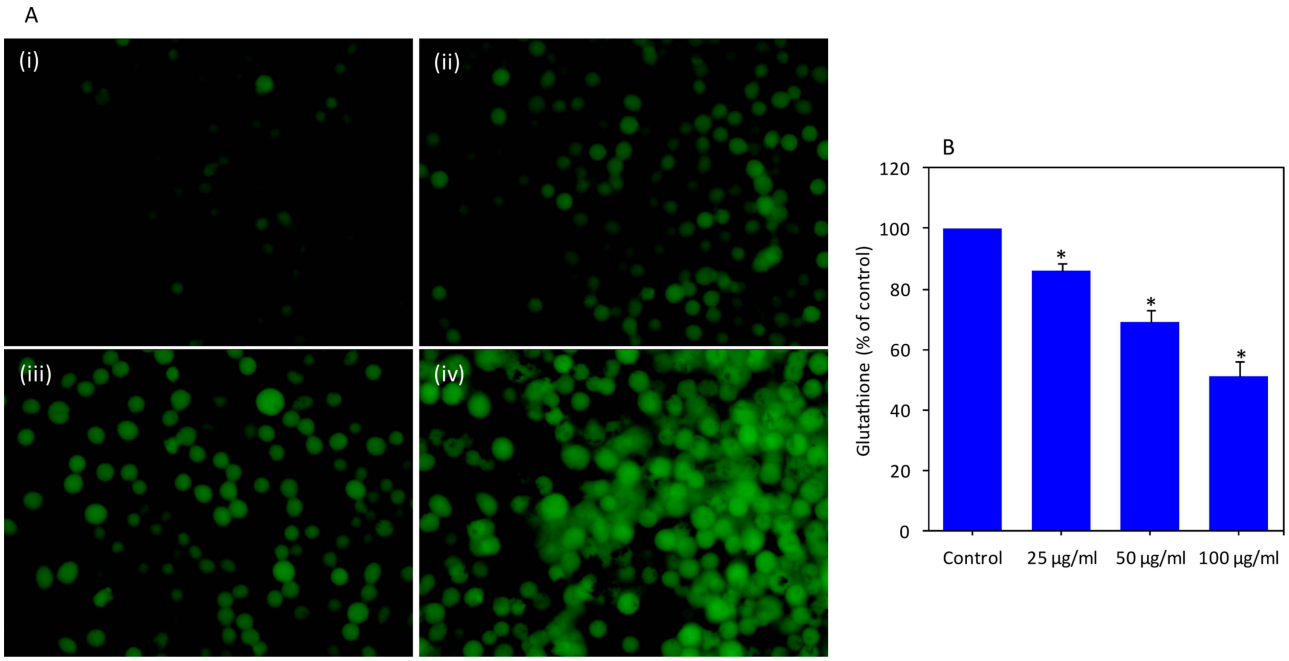

Fig. 3. Dose-dependent induction of oxidative stress in HepG2 cells after Ni NPs exposure. (A) Induction of ROS level: (i) control, (ii) 25 μg/mL, (iii) 50 μg/mL, and (iv) 100 μg/mL. Fluorescence microscope images are the representative of three identical experiments. (B) Depletion of GSH level. Data represented are mean ± SD of three identical experiments made in three replicate. *Statistically significant difference as compared to control ($p < 0.05$). [Color figure can be viewed in the online issue, which is available at wileyonlinelibrary.com.]

Nickel Nanoparticles Induced Reactive Oxygen Species Generation

Intracellular ROS production has been suggested to be signaling molecule for the initiation and execution of apoptosis (Nel, 2006; Ott et al., 2007). Therefore, we examined the effect of Ni NPs on ROS generation in HepG2 cells. Fluorescent microscopy data revealed that Ni NPs (25–100 μg/mL) induced the intracellular production of ROS dose-dependently [Fig. 3(A)].

Nickel Nanoparticles Depleted Glutathione Level

The depletion of GSH and indicative of ROS generation have also been implicated in oxidative damage of cellular macromolecules like protein, DNA and RNA (Ahamed et al., 2010; Akhtar et al., 2012). We also evaluated the GSH level in HepG2 cells treated with Ni NPs at concentrations of 25, 50, and 100 μg/mL for 24 h. Results showed that GSH level was depleted with the concentrations Ni NPs [Fig. 3(B)].

Nickel Nanoparticles Decreased Mitochondrial Membrane Potential

It is well-known that during apoptosis the mitochondrial membrane potential (MMP) of cells decreases (Sharma et al., 2012). Ni NPs induced differences in MMP in HepG2 cells were recorded in terms of fluorescence intensity of mitochondria specific dye Rh-123. A dose-dependent decrease in Rh-123 fluorescent intensity was observed in HepG2 cells exposed to different concentrations of Ni NPs (25–100 μg/mL) (Fig. 4).

Alterations in Cell Cycle Progression After Nickel Nanoparticles Exposure

ROS generation in Ni NPs treated cells indicated the possibility of DNA damage and apoptosis where the early effect will be evidenced in cell cycle progression. Cells with damaged DNA will accumulate in gap1 (G1), DNA synthesis (S), or in gap2/mitosis (G2/M) phase. Cells with irreversible damage will undergo apoptosis, giving rise to accumulation of cells in subG1 phase (Ishikawa et al., 2006). Thus toxicity studies were further extended to cell cycle analysis to detect parameters such as apoptosis. Our flow-cytometric analysis of cell cycle revealed the induction of apoptosis in HepG2 cells upon treatment with different concentrations of Ni NPs (25–100 μg/mL) [Fig. 5(A)]. Ni NPs at the highest concentration of 100 μg/mL resulted in the appearance of significant 13.5% cells in SubG1 phase in treated cells as compared to the 5.8% in control group [Fig. 5(B)]. Significant decline in G2/M phase was also evident from the appearance of 21.6, 18.3, and 15.7% of cells in G2/M phase

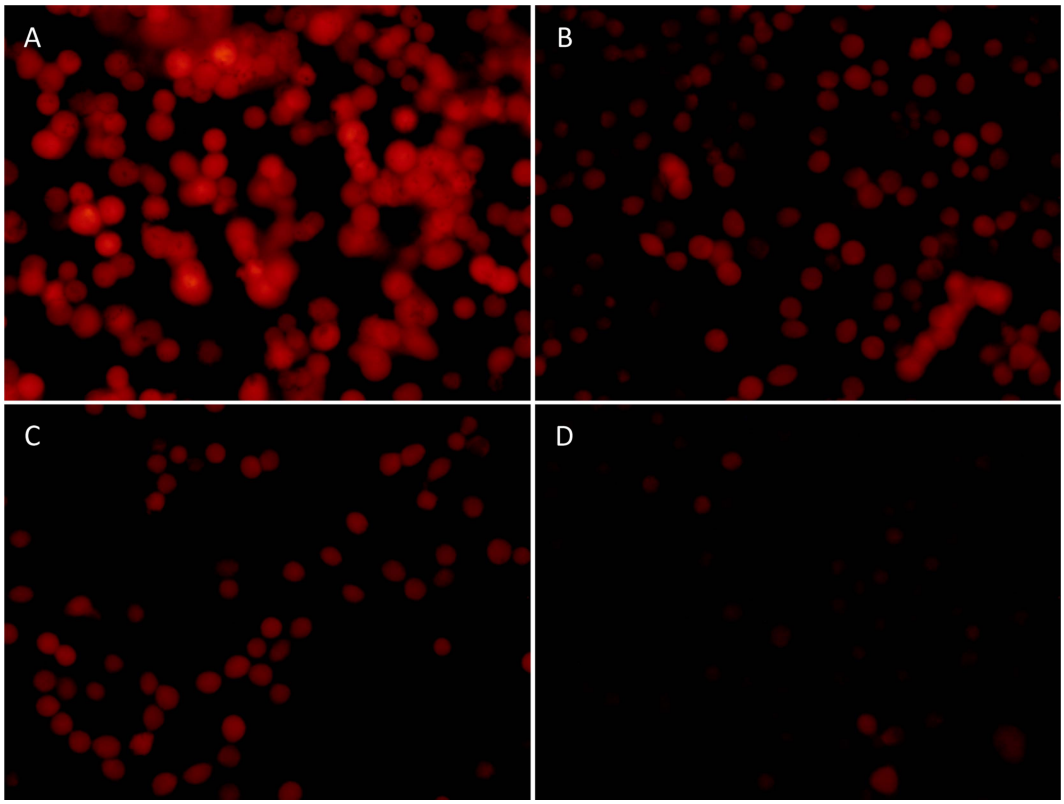

Fig. 4. Dose-dependent induction of mitochondria membrane potential in HepG2 cells after Ni NPs exposure. (A) Control, (B) 25 μg/mL, (C) 50 μg/mL, and (D) 100 μg/mL. Fluorescence microscope images are the representative of three identical experiments. [Color figure can be viewed in the online issue, which is available at wileyonlinelibrary.com.]

treated with 25, 50, and 100 μg/mL Ni NPs, respectively versus 25.6% of cells in G2/M phase in the control [Fig. 5(B)].

Alterations in the Expressions of mRNA of Apoptotic Genes After Nickel Nanoparticles Exposure

Quantitative real-time PCR was used to analyze the mRNA levels of apoptotic genes (p53, bax, bcl-2, and caspase-3) in HepG2 cells exposed to Ni NPs at the concentrations of 25, 50, and 100 μg/mL for 24 h. We observed that Ni NPs significantly altered the expressions of mRNA of these genes dose-dependently. The mRNA expressions of tumor suppressor gene p53 and apoptotic genes bax & caspase-3 were upregulated while the expression of anti-apoptotic gene bcl-2 was down-regulated in Ni NPs treated cells as compared to controls (Fig. 6) ($p < 0.05$ for each).

Nickel Nanoparticles Induced Caspase-3 Enzyme Activity and DNA Fragmentation

We observed that activity of caspase-3 enzyme was induced by Ni NPs and degree of induction was concentration-dependent [Fig. 7(A)]. We further analyzed the DNA profiles of the cells treated with various concentrations of Ni NPs for 24 h. Results revealed that in control cells the DNA was not fragmented, whereas the cells treated with Ni NPs had started the apoptotic process, as evident by DNA fragmentation [Fig. 7(B)].

DISCUSSION

Ni NPs are manufactured worldwide for multiple applications including catalysts, sensors and energy storage devices (Zhang et al., 1998). In addition, these NPs are also used as catalysts for the generation of some types of carbon nanotubes (Donaldson et al., 2006). Any product that contains carbon nanotubes, including medical devices, may contain residual Ni NPs. Although these catalyst residues appear to be encapsulated inside the carbon shells, a fraction is typically bioavailable (Liu et al., 2007). These broad applications of Ni NPs are accompanied by limited safety regulations and toxicological data (Pietruska et al., 2011). Recently, a case study confirms that Ni NPs are indeed a toxicological hazard that can cause acute and fatal disease in humans (Phillips et al., 2010). These authors re-examined a case described in 1994 from a pathology perspective. The subject, a 38-year-old previously healthy male, inhaled Ni NPs while spraying Ni onto bushes for turbine bearings using a metal arc process. He died 13 days after being

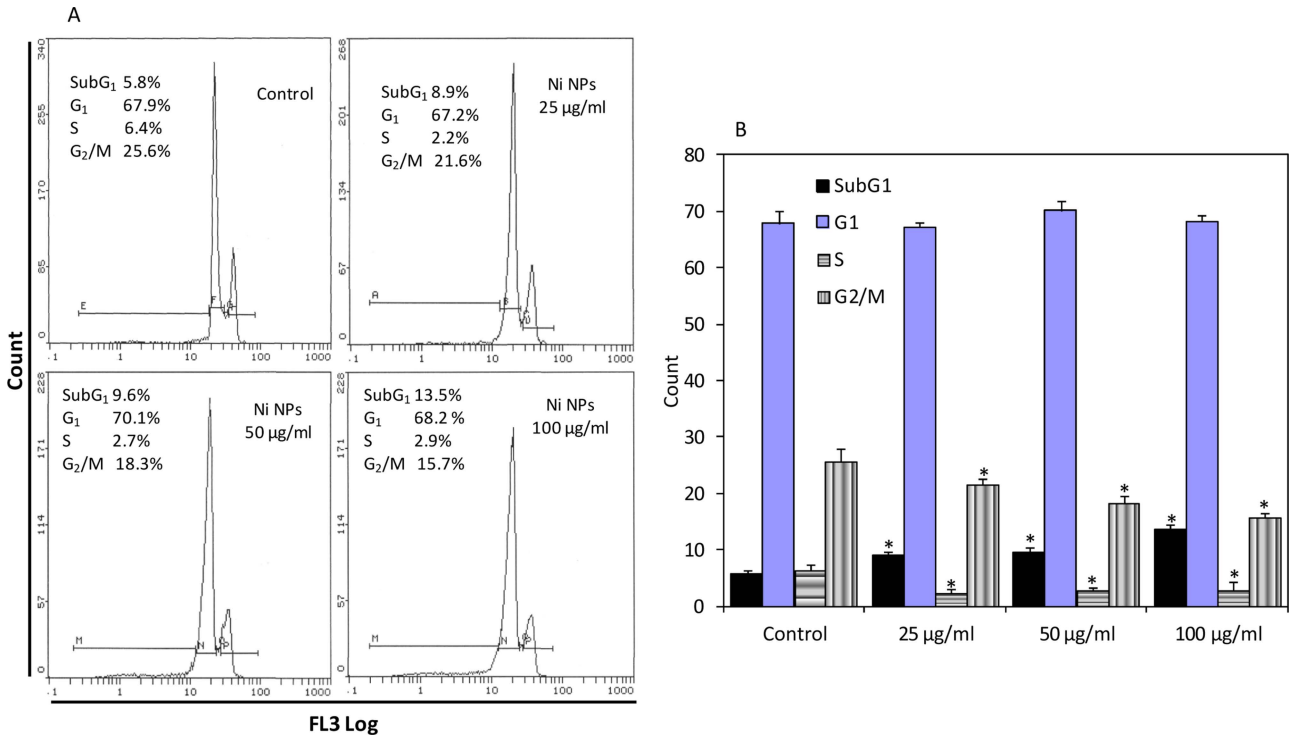

Fig. 5. Cell cycle analysis of HepG2 cells after Ni NPs exposure. (A) Representative flow cytometric image from single experiment exhibiting changes in the progression of cell cycle in HepG2 cells after Ni NPs exposure. G1, S, and G2/M in each micrograph represent the percentage of cells present in normal phases of cell cycle whereas SubG1 represents percentage of cells that undergone apoptosis. (B) Each histogram represents mean ± SD values of different phases of cell cycle obtained from three identical experiments made in three replicate. *Statistically significant difference as compared to control ($p < 0.05$). [Color figure can be viewed in the online issue, which is available at wileyonlinelibrary.com.]

exposed and the cause of death at autopsy was adult respiratory distress syndrome. Ni NPs (<25 nm) were identified in lung macrophages and high levels of Ni were measured in his urine and kidneys showed evidence of acute tubular necrosis. In keeping with expert opinion, animal and *in vitro* models, the NPs may affect organs other than the lungs. This prompted us to investigate the toxic potential of Ni NPs. We found that exposure of Ni NPs to human liver cells (HepG2) cause cytotoxicity and oxidative stress. Ni NPs were also found to induce apoptosis in HepG2 cells evidenced by higher MMP, altered expression of p53, bax, bcl-2, and caspase-3 genes and DNA fragmentation along with cell cycle arrest in SubG1 phase.

MTT and NRU results revealed that the Ni NPs (size: 28 nm) reduce the viability of HepG2 cells in dose-dependent manner in the concentration range of 25–100 µg/mL. Ni NPs at the concentration of ≤10 µg/mL did not produce significant reduction in HepG2 cells viability. However, our previous study has shown that minimum concentration of Ni NPs (size: 65 nm) that cause cytotoxicity in human lung epithelial (A549) cells was 2 µg/mL. These results suggested that human liver is more resistible to Ni NPs exposure as compared to lungs. MTT and NRU assays represent the damage in mitochondrial and lysosomal membranes, respectively that eventually triggers the cell death. These assays served as sensitive and integrated measure of cell integrity and inhibition of cell proliferation. These results are consistent with the observed low MMP and high SubG1 cell population during cell cycle progression in cells exposed to Ni NPs. Appearance of sub-G1 peak with increasing dose of Ni NPs suggested the possible involvement of apoptotic pathway, triggered by alteration in mitochondrial and lysosome functions (Nicoletti et al., 1991; Ravi et al., 2010). A recent study suggested that mitochondrial events of apoptosis involve opening of a pore in the inner mitochondrial membrane, referred as mitochondrial permeability transition pore (MPTP), and loss of MMP (Kitsis and Molkentin, 2010). This is consistent with the effects of Ni NPs observed in the MTT assay that suggested mitochondrial dysfunction. Opening of the MPTP results in mitochondrial swelling and rupture of outer mitochondrial membrane during apoptosis. This subsequently results in release of apoptogens that likely engage the components of apoptosis machinery to further enhance cell death (Kitsis and Molkentin, 2010). Damage to lysosomal membranes is known to release lysosome protease into intracellular spaces, which affects the neighbor cells, and triggers cell death due to apoptosis (Leist and Jaattela, 2001).

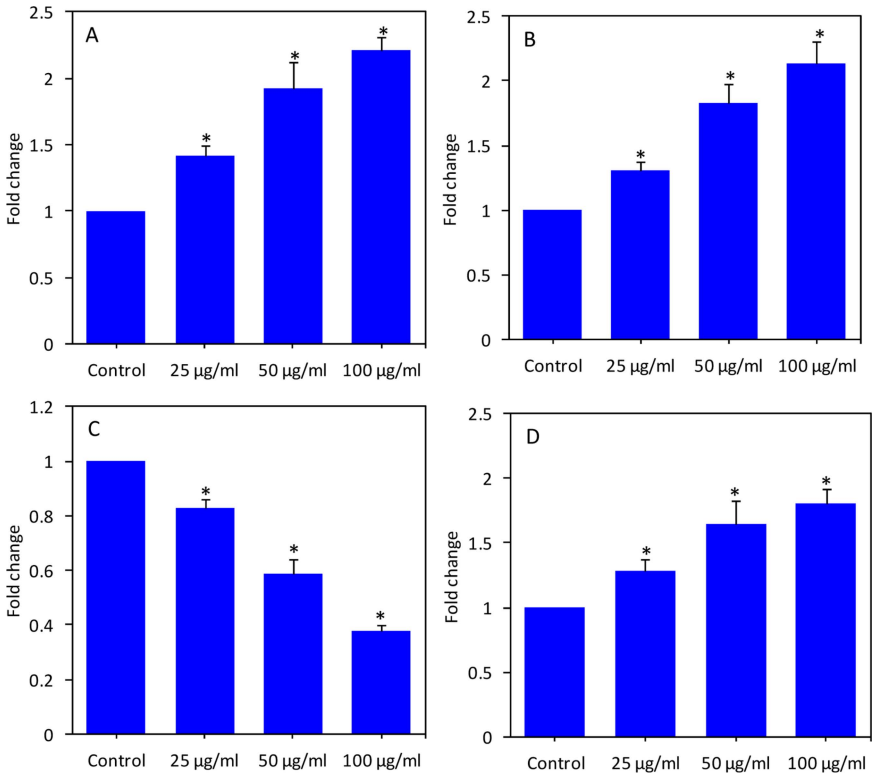

Fig. 6. Quantitative real-time PCR analysis of mRNA levels of apoptotic genes in HepG2 cells after Ni NPs exposure. (A) p53, (B) bax, (C) bcl-2, and (D) caspase-3. Data represented are mean ± SD of three identical experiments made in three replicate. *Statistically significant difference as compared to control ($p < 0.05$). [Color figure can be viewed in the online issue, which is available at wileyonlinelibrary.com.]

Due to small size and large surface area, NPs are generally thought to induce ROS generation and cellular oxidative stress (Nel et al., 2006). ROS such as superoxide anion, hydroxyl radical and hydrogen peroxide provoke a variety of physiological and cellular events including inflammation, DNA damage and apoptosis (Asharani et al., 2009; Siddiqui et al., 2012; Ahamed, 2013). There have been increasing scientific evidences that indicate the role ROS in various human diseases including cancer (Benz and Yau, 2008; Jomova and Valko, 2011). In the present investigation, we observed that ROS level was higher while the antioxidant GSH level was lower concentration-dependently in Ni NPs treated HepG2 cells. These results are in agreement with our previous reports where nickel based NPs induced ROS mediated toxicity in cultured human cells (Ahamed, 2011; Ahamed et al., 2011; Siddiqui et al., 2012; Ahamed et al., 2013).

The p53 protein is regarded as the guardian of the cell genome is able to activate cell cycle checkpoints, DNA repair and apoptosis to maintain stability of genome (Sherr, 2004). In the presence of cellular stress, p53 triggers cell cycle arrest to provide time for the damage to be repaired or self-mediated apoptosis (Farnebo et al., 2010). Studies have shown that the most of the inorganic NPs induce apoptosis through the mitochondrion-mediated pathway (Choi et al., 2008; Sharma et al., 2012), in which mitochondrial permeability transition is firstly promoted, followed by the release of apoptogenic factors such as cytochrome c and apoptosis-inducing factor, the activation of initiator caspase-9 and effector caspase-3. Also, the Bcl-2 family proteins have been considered as critical regulators of the mitochondria-mediated apoptosis by functioning as either promoters (e.g., bax) or inhibitors (e.g., bcl-2) of the cell death process (Yao et al., 2008; Youle and Strasser, 2008; Chougule et al., 2011). In this study, quantitative real-time PCR results demonstrated mRNA of cell cycle checkpoint protein p53 and apoptotic proteins (bax and caspase-3) were upregulated while the expression of anti-apoptotic protein bcl-2 was down-regulated in HepG2 cells after Ni NPs exposure. In agreement with mRNA data we also found that Ni NPs induce activity of caspase-3 enzyme and DNA fragmentation in HepG2 cells.

In conclusion, we observed that Ni NPs induce cytotoxicity and oxidative stress in human liver cells and degree of induction was concentration-dependent. Cell cycle analysis of HepG2 cells treated with Ni NPs exhibited significant increase of apoptotic cell population in subG1 phase. Higher activity caspase-3 enzyme and DNA fragmentation due to Ni NPs exposure was also suggested the apoptotic response of Ni NPs. Upregulation of cell cycle checkpoint gene p53

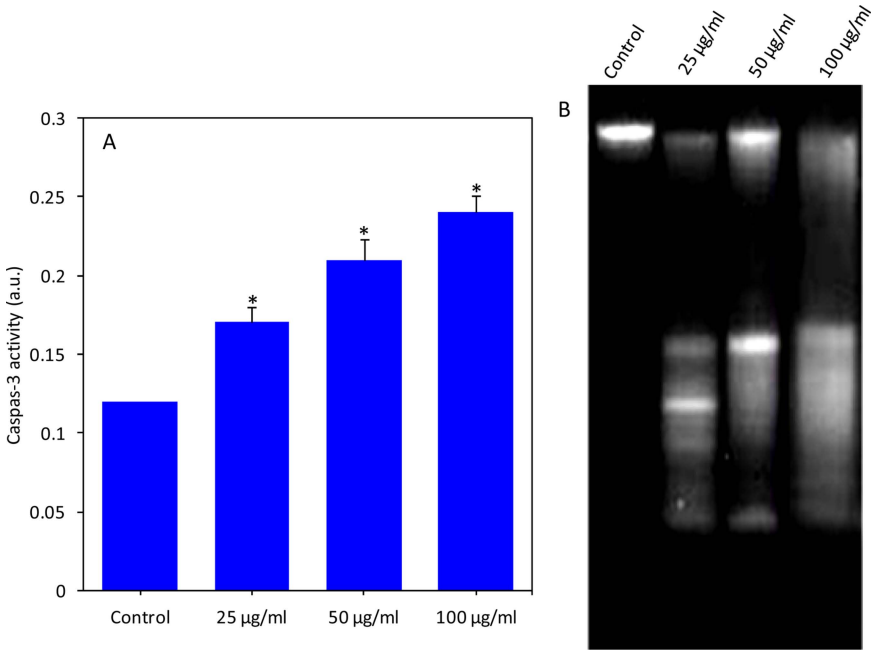

Fig. 7. Dose-dependent induction of caspase-3 enzymes activity and DNA fragmentation in HepG2 cells after Ni NPs exposure. (A) Caspase-3 enzyme activity and (B) Apoptotic DNA fragmentation. Data represented are mean ± SD of three identical experiments made in three replicate. *Statistically significant difference as compared to control ($p < 0.05$). [Color figure can be viewed in the online issue, which is available at wileyonlinelibrary.com.]

and bax/bcl-2 ratio along with a concomitant loss of MMP suggested that Ni NPs induced apoptosis in HepG2 cells, which was mediated through mitochondrial pathway. This study suggests that industrial and commercial applications Ni NPs should be more carefully and thoroughly assessed as to their potential hazardous effects to human health.

REFERENCES

Ahamed M. 2011. Toxic response of nickel nanoparticles in human lung epithelial A549 cells. Toxicol In Vitro 25:930–936.

Ahamed M. 2013. Silica nanoparticles induced cytotoxicity, oxidative stress and apoptosis in A549 and A431 cells. Human Exp Toxicol 32:186–195.

Ahamed M, AlSalhi MS, Siddiqui MKJ. 2010. Silver nanoparticle applications and human health. Clin Chim Acta 411:1841–1848.

Ahamed M, Akhtar MJ, Siddiqui MA, Ahmad J, Musarrat J, Al-Khedhairy AA, Alrokayan SA. 2011. Oxidative stress mediated apoptosis induced by nickel ferrite nanoparticles in cultured A549 cells. Toxicology 283:101–108.

Ahamed M, Alhadlaq HA, Khan MAM, Akhtar MJ. 2013. Selective killing of cancer cells by iron oxide nanoparticles mediated through reactive oxygen species via p53 pathway. J Nanopart Res 15:1225.

Ahmad J, Ahamed M, Akhtar MJ, Alrokayan SA, Siddiqui MA, Musarrat J, Al-Khedhairy AA. 2012. Apoptosis induction by amorphous silica nanoparticles mediated through reactive oxygen species generation in human liver cell line HepG2. Toxicol Appl Pharmacol 259:160–168.

Akhtar MJ, Ahamed M, Kumar S, Ahmad J, Khan MAM and Alrokayan SA. 2012. Zinc oxide nanoparticles selectively induces apoptosis in cancer cells through reactive oxygen species. Int J Nanomed 7:845–857.

Andrew D, Maynard EK. 2005. Airborne nanostructured particles and occupational health. J Nanopart Res 587:14.

Asharani PV, Mun GK, Hande MP, Valiyaveettil S. 2009 Cytotoxicity and genotoxicity of silver nanoparticles in human cells. ACS Nano 3:279–290.

Benz CC, Yau C. 2008. Ageing, oxidative stress and cancer: Paradigms in parallax. Nat Rev Cancer 8:875–879.

Berasain C, Garcia-Trevijano ER, Castillo J, Erroba E, Santamaria M, Lee DC. 2005. Novel role for amphiregulin in protection from liver injury. J Biol Chem 280:19012–19020.

Borenfreund E, Puerner JA. 1984. A simple quantitative procedure using monolayer cultures for cytotoxicity assays. J Tissue Culture Method 9:7–9.

Bradford MM. 1976. A rapid and sensitive method for the quantitation of microgram quantities of protein utilizing the principle of protein-dye binding. Anal Biochem 72:248–254.

Cavallo D, Ursini CL, Setini A, Chianese C, Piegari P, Perniconi B, Iavicoli S. 2003. Evaluation of oxidative damage and inhibition of DNA repair in an in vitro study of nickel exposure. Toxicol In Vitro 17:603–607.

Chandra D, Ramana KV, Wang L, Christensen BN, Bhatnagar A, Srivastava SK. 2002. Inhibition of fiber cell globulization and

hyperglycemia-induced lens opacification by aminopeptidase inhibitor bestatin. Invest Ophth Vis Sci 43:2285–2292.

Chen Z, Meng H, Yuan H, Xing G, Chen C, Zhao F, Wang Y, Zhang C, Zhao C. 2007. Identification of target organs of copper nanoparticles with ICPMS technique. J Radioanal Nucl Chem 272:599–603.

Choi BH, Kim W, Wang QC, Kim DC, Tan SN. 2008. Kinetin riboside preferentially induces apoptosis by modulating Bcl-2 family proteins and caspase-3 in cancer cells. Cancer Lett 261: 37–45.

Chougule M, Patel AR, Sachdeva P, Jackson T, Singh M. 2011. Anticancer activity of noscapine, an opioid alkaloid in combination with cisplatin in human non-small cell lung cancer. Lung Cancer 71:271–282.

Clancy HA, Costa M. 2012. Nickel: A pervasive carcinogen. Future Oncol 8:1507–1509.

Darzynkiewicz Z, Bruno S, Bino G. 1992. Features of apoptosis cells measured by flow cytometry. Cytometry 13:795–608.

Donaldson K, Aitken R, Tran L, Stone V, Duffin R, Forrest G. 2006. Carbon nanotubes: A review of their properties in relation to pulmonary toxicology and workplace safety. Toxicol Sci 92:5–22.

Farnebo M, Bykov VN, Wiman KG. 2010. The p53 tumor suppressor: A master regulator of diverse cellular processes and therapeutic target in cancer. Biochem Biophys Res Commun 396:85–89.

Guo D, Wu C, Li X, Jiang H, Wang X, Chen B. 2008. In vitro cellular uptake and cytotoxic effect of functionalized nickel nanoparticles on leukemia cancer cells. J Nanosci Nanotechnol 8:2301–2307.

Ishikawa K, Ishii H, Saito T. 2006. DNA damage-dependent cell cycle checkpoints and genomic stability. DNA Cell Biol 25: 406–411.

Ispas C, Andreescu D, Patel A, Goia DV, Andreescu S, Wallace KN. 2009. Toxicity and developmental defects of different sizes and shape nickel nanoparticles in zebrafish. Environ Sci Technol 43:6349–6356.

Jomova K, Valko M. 2011. Advances in metal-induced oxidative stress and human disease. Toxicology 283:65–87.

Kasprzak KS, Sunderman FW Jr, Salnikow K. 2003. Nickel carcinogenesis. Mutat Res 533:67–97.

Kim YS, Kim JS, Cho HS, Rha DS, Kim JM, Park JD, Choi BS, Lim R, Chang HK, Chung YH, Kwon IH, Jeong J, Han BS, Yu IJ. 2008. Twenty eight day oral toxicity, genotoxicity, and gender-related tissue distribution of silver nanoparticles in Sprague–Dawley rats. Inhal Toxicol 20:575–583.

Kitsis RN, Molkentin JD. 2010. Apoptotic cell death nixed by an ER–mitochondrial necrotic pathway. Proc Nat Acad Sci USA 107:9031–9032.

Leist M, Jaattela M. 2001. Four deaths and a funeral: From caspases to alternative mechanisms. Nat Rev Mol Cell Biol 2: 589–598.

Liu X, Gurel V, Morris D, Murray DW, Zhitkovich A, Kane AB, Hurt RH. 2007. Bioavailability of nickel in single-wall carbon nanotubes. Adv Mater 19:2790–2796.

Magaye R, Zhao J. 2012. Recent progress in studies of metallic nickel and nickel-based nanoparticles genotoxicity and carcinogenicity. Environ Toxicol Pharmacol 34:644–650.

Mossman T. 1983. Rapid colorimetric assay for cellular growth and survival: Application to proliferation and cytotoxicity assays. J Immunol Methods 65:55–63.

Murdock RC, Braydich-Stolle L, Schrand AM, Schlager JJ, Hussain SM. 2008. Characterization of nanomaterial dispersion in solution prior to in vitro exposure using dynamic light scattering technique. Toxicol Sci 101:239–253.

Nel A, Xia T, Madler L, Li N. 2006. Toxic potential of materials at the nanolevel. Science 311:622–627.

Nicoletti I, Migliorati G, Pagliacci MC, Grignani F, Riccardi C. 1991. A rapid and simple method for measuring thymocyte apoptosis by propidium iodide staining and flow cytometry. J Immunol Methods 139:271–279.

Oller AR, Costa M, Oberdorster G. 1997. Carcinogenicity assessment of selected nickel compounds. Toxicol Appl Pharmacol 143:152–166.

Ott M, Gogvadze V, Orrenius S, Zhivotovsky B. 2007. Mitochondria, oxidative stress and cell death. Apoptosis 12:913–922.

Patterson AL. 1939. The Scherrer formula for X-ray particle size determination. Phys Rev 56:978–982.

Phillips JI, Green FY, Davies JA, Murray J. 2010. Pulmonary and systemic toxicity following exposure to nickel nanoparticles. Am J Ind Med 53:763–767.

Pietruska JR, Liu X, Smith A, McNeil K, Weston P, Zhitkovich A, Hurt R, Kane AB. 2011. Bioavailability, intracellular mobilization of nickel, and HIF-1 activation in human lung epithelial cells exposed to metallic nickel and nickel oxide nanoparticles. Toxicol Sci 124:138–148.

Ravi S, Chiruvella KK, Rajesh K, Prabhu V, Raghavan SC. 2010. 5-Isopropylidene-3-ethyl rhodanine induce growth inhibition followed by apoptosis in leukemia cells. Eur J Med Chem 45: 2748–2752.

Sharma V, Anderson D, Dhawan A. 2012. Zinc oxide nanoparticles induce oxidative DNA damage and ROS-triggered mitochondria mediated apoptosis in human liver cells (HepG2). Apoptosis 17:852–870.

Sherr CJ. 2004. Principles of tumor suppression. Cell 11:235–246.

Siddiqui MA, Kashyap MP, Kumar V, Al-Khedhairy AA, Musarrat J, Pant AB. 2010. Protective potential of trans-resveratrol against 4-hydroxynonenal induced damage in PC12 cells. Toxicol In Vitro 24:1592–1598.

Siddiqui MA, Ahamed M, Ahmad J, Khan MAM, Musarrat J, Al-Khedhairy AA, Alrokayan SA. 2012. Nickel oxide nanoparticles induce cytotoxicity, oxidative stress and apoptosis in cultured human cells that is abrogated by the dietary antioxidant curcumin. Food Chem Toxicol 50:641–647.

Sivulka DJ. 2005. Assessment of respiratory carcinogenicity associated with exposure to metallic nickel: A review. Regul Toxicol Pharmacol 43:117–133.

Wang B, Feng W, Wang M, Wang T, Gu T, Zhu M, Ouyang H, Shi J, Zhang F, Zhao F, Chai Z, Wang H, Wang J. 2008. Acute

toxicological impact of nano- and submicro-scaled zinc oxide powder on healthy adult mice. J Nanopart Res 10:263–276.

Wang H, Joseph JA. 1999. Quantifying cellular oxidative stress by dichlorofluorescin assay using microplate reader. Free Radic Biol Med 27:612–616.

Wang H, Kou X, Zhang J, Li J. 2008. Large scale synthesis and characterization of Ni nanoparticles by solution reduction method. Bull Mater Sci 31:97–100.

Yao JC, Jiang ZZ, Duan WG, Huang JF, Zhang LY, Hu L, He L, Li F, Xiao Y, Shu B, Liu C. 2008. Involvement of mitochondrial pathway in triptolide-induced cytotoxicity in human normal liver L-02 Cells. Biol Pharm Bull 31:592–597.

Youle RJ, Strasser A. 2008. The BCL-2 protein family: Opposing activities that mediate cell death. Nat Rev Mol Cell Biol 9: 47–59.

Zhang Q, Kusaka Y, Zhu X, Sato K, Mo Y, Donaldson K. 1998. Differences in the extent of inflammation caused by intratracheal exposure to three ultrafine metals: Role of free radicals. J Toxicol Environ Health A 53:423–438.

Zhang Q, Kusaka Y, Zhu X, Sato K, Mo Y, Kluz T, Donaldson K. 2003. Comparative toxicity of standard nickel and ultrafine nickel in lung after intratracheal instillation. J Occup Health 45: 23–30.

Zhang Y, Jiang L, Jiang L, Geng C, Li L, Shao J, Zhong L. 2011. Possible involvement of oxidative stress in potassium bromate-induced genotoxicity in human HepG2 cells. Chem Biol Int 189:186–191.

Zhao J, Bowman L, Zhang X, Shi X, Jiang B, Castranova V, Ding M. 2009. Metallic nickel nano- and fine particles induce JB6 cell apoptosis through a caspase-8/AIF mediated cytochrome c-independent pathway. J Nanobiotechnol 7:13.

Zou J, Chen Q, Jin X, Tang S, Chen K, Zhang T, Xia X. 2011. Olaquindox induces apoptosis through the mitochondrial pathway in HepG2 cells. Toxicology 285:104–133.